

Interactive comment on “Short Communication: Challenges and Applications of Structure-from-Motion Photogrammetry in a Physical Model of a Braided River” by P. Leduc et al., esurf-2018-45

We thank the two referees for their comments. Our responses below are organised to respond to each review in sequence.

The following changes have been made :

- New references have been added
- Technical details have been added (interpolation, laser scan,...)
- The wording error/precision is changed for section 3

Answers are in italic font.

Anonymous Referee 1

The introduced study describes the application of SfM to measure DEMs of flumes in laboratory setups. Images for SfM are acquired in sequence and resulting DEMs are compared to each other and to TLS data. The manuscript is well written and clearly structured. Methods and results are illustrated sufficiently. However, there are some concerns, which should be addressed before the manuscript can be accepted for publication. The novelty of the introduced results seems to be not very high because many of the mentioned findings, e.g. regarding doming effects or the impact of image quality, are already discussed in other work but just for different scales (e.g. see James et al. 2017, Mosbrucker et al. 2017). The generation of a very high number of DEMs used for DoD calculation is interesting and could be novel if the potential of such data regarding the expected new insights into investigating fluvial processes would be displayed and discussed. Furthermore, the processing of such data to extract the relevant information needed to assess the processes would be of interest. Regarding the references, some more literature should be included concerning the utilization of SfM in laboratory setups in geomorphological applications. For instance, Galland et al. 2015 use SfM and time-lapse imagery in geological experiments with sub-mm accuracy, Kaiser et al. 2018 as well achieve sub-mm accuracy when they perform close-range SfM measurements to detect soil surface changes, and Balaguer-Puiga et al. 2017 use SfM to measure soil erosion at micro-plots in the lab. Furthermore, some concerns exist regarding the usage of two sets of images to estimate the error in this study due to the missing consideration of spatial correlation of errors. Please, see a more detailed description of the raised concerns in the specific comments section.

Thank you for your comments. Indeed, the SfM is providing a large amount of data but the main focus of the paper is SfM application to laboratory flumes rather than morphology studies. Three papers have been recently published based on the data-set [Peirce et al., 2018a,b, Middleton et al., 2018] which provide examples of applications to analysis of relevant fluvial processes. We added to the paper example of results and geomorphic analysis. The comments regarding references will be addressed on the specific comments.

S. Peirce, P. Ashmore, and P. Leduc. The variability in the morphological active width: Results from physical models of gravel-bed braided rivers. Earth Surface Processes and Landforms, 43(11):2371–2383, may 2018a. doi: 10.1002/esp.4400.

S. Peirce, P. Ashmore, and P. Leduc. Evolution of grain size distributions and bed mobility during hydrographs in gravel-bed braided rivers. Earth Surface Processes and Landforms, sep 2018b. doi: 10.1002/esp.4511.

L. Middleton, P. Ashmore, P. Leduc, and D. Sjogren. Rates of planimetric change in a proglacial gravel-bed braided river: field measurement and physical modeling. Earth Surface Processes and Landforms, oct 2018. doi: 10.1002/esp.4528.

Specific comments:

p. 1 l. 14-19: The DEMs are not mainly limited by the image quality. There are further important error sources leading to potential systematic errors (e.g. dome effects) as well as to random errors, which are highly spatially correlated, amongst others due to the right choice of parameters and their setting (see James et al. 2017).

We noticed a doming effect during our primary tests but the camera calibration and parameter adjustments reduced it and we didn't notice any obvious systematic error afterwards. Further details have been added to the paper based on the mentioned references.

p. 1 l. 21: More literature regarding SfM and fluvial morphology should be introduced, e.g. Javernick et al. 2014 or Woodget et al. 2015. These authors are one of the first to introduce SfM (in combination with UAV) to fluvial morphology.

The mentioned references have been added to the paper. Note that we limited the review to those applications specifically related to close-range applications in laboratory flumes with fixed geometry which is the focus of the paper, rather than more broadly to fluvial morphology primarily acquired from drones in the field which introduce other analytical issues less relevant to our work.

p. 2 l. 18-20: I am afraid that I do not understand in what sequence the image pairs were acquired. Were the two sets of images taken during one acquisition (thus both images in short sequence at each position) or were two acquisitions performed in sequence (thus images once during first interval and once again during second interval)? This information would be important because if the images were acquired from the same position just in sequence their suitability to assess DEM errors would be questionable because acquisition geometry would be almost identical and thus not much change expected in the images. Generally, if camera geometry and surface texture conditions (also considering lighting) for both sets of digital images are similar, not much information regarding accuracy, utilizing DoD differencing, can be expected because errors are spatially highly correlated (James et al. 2017). The raised concern regarding spatial error correlation also relates to p. 4 l. 7-9.

The 2 sets of pictures were taken on the same surface but during 2 different acquisitions. The second set of pictures was taken after the first one was completely done, which means they are two separate traverses of the camera trolley along the flume length. The 2 sets of pictures don't have the same number of pictures, mean overlap, or exact start and end locations. This gives at least some estimate of the precision and repeatability of the survey. Details have been added to the paper.

chapter 3.1: Why did the authors not exclude some of the coded targets (because many are given) during the bundle adjustment so these targets could be considered as check points and thus used for accuracy assessment of each SfM surface and camera geometry reconstruction?

We contemplated this but some targets weren't well detected on every DEM, especially during the early experiments. We preferred to keep the entire target set and try a different way to estimate the error and precision using the model surfaces rather than a few targets.

p. 4. L. 3: What TLS has been used? What accuracy and resolution does the device provide?

The scanner is a hand-held Exascan scanner from Creaform for which distance to the surface could be kept relatively constant rather than the radial distance effects of TLS at very close range. The resolution is 0.050 mm and the accuracy up to 0.040 mm. This information has been added to the paper.

p. 4 L. 9-10: The usage of just one value (mean of entire DoD) is not able to describe the spatially variable error, e.g. due to potential tilting. How is this considered for the decision of the DEM?

Indeed, the mean value isn't able to describe a potential tilting; nevertheless we didn't notice any consistent spatial variability (see figure below) on the DoD or a tilting on the cross section or longitudinal profiles.

p. 4 l. 10-12: How certain are the authors that surface changes to the previous time interval are not conflicting the decision for the most suitable DEM of the subsequent interval?

The two DEMs for each time interval are generated by the same process each time. They are therefore detecting the same changes from the previous DEM so that both DoDs contain the (same) real morphological change as well as the DEM error. Our method was intended to include potential differences due to DEM error and to select the DEM for which the ‘global’ errors were smallest. We are assuming that the DEM error will add topographic bed variation and so increase the mean value.

p. 6 l. 3: Already James et al. 2017b illustrate the importance of GCP number and distribution for the DEM quality. Maybe refer to their work.

We now refer to their work.

p. 6 l. 4-8: Please, refer to James and Robson 2014 regarding doming effect because they perform extensive simulations to explain the causes (i.e. image geometry) of doming errors and already show that convergent images improve data accuracy.

We now refer to their work.

p. 6. l. 9: Please, refer to Mosbrucker et al. 2016 who explain very detailed the importance of image quality for DEMs derived with SfM.

We now refer to their work.

p. 6. l. 11: Why is the fixed focal length essential during low light conditions and low texture? The interior geometry does not influence these circumstances. The fixed focal length is important regarding a reliable camera self-calibration. Good texture is essential for feature extraction and matching but not influenced by the stability of the focal length. To improve texture e.g. aperture and/or exposure time should be adapted (see Mosbrucker et al. 2016 for much more detail).

We have rephrased this to reflect the point. The fixed focal length is useful at close range (not relevant for UAV imagery) to keep the focus as sharp and consistent as possible which has a major effect on the quality of the results if low light affects the auto-focus.

p. 7 l. 1-2: How was the DEM interpolated from the dense point cloud? PhotoScan offers different options potentially influencing the final DEM.

We use the Photoscan interpolation (enabled option).

chapter 5.2: How certain are the authors that indeed water surface has been detected/ reconstructed with SfM? The “water surface” could also be the result of some interpolation artefact in PhotoScan because the water is moving and thus feature matching in this area from images captured in (although very short) temporal sequence is unreliable. Did the authors perform some independent reference measurement of the water depth to confirm the SfM results?

The water surface is not directly detected with SfM. We are actually assuming that water surface disturbs the elevation signal. We compared the DEM created with the water flow, with that from the dry bed DEM and identified cells with elevation differences above a threshold which we are assuming represent the water extent. We are not using the real water running DEM but only the binary maps water/dry resulting from the DoD between the dry and wet DEM. To estimate the water depth, we use the dry topography given the position of the water edge and extent. Measuring the real water depth is quite difficult except for a few local ‘spot checks’ but we are able to compare the water surface extent with that visually apparent on the images. This is effective in the case of wide, shallow braided channels but may be less effective for other river morphology. More details have been added to the paper.

p. 8 l. -10: I am afraid that I do not understand what is meant by cross-sectional scale? Did the authors extract water levels at each cross section? If yes, how were the cross-sections extracted and what would be the spatial resolution?

The point is that we assume that the water surface is straight for any given cross-section of the river between points where the water surface intersects the bed topography (Fig 6). The water surface estimation

is done for each cross-section so that the spatial resolution is the same as that of the DEM.

chapter 5.3: Maybe, the authors could also test the usage of the retrieved 3D data with SfM to extract grain sizes directly from roughness estimates calculated with the DEMs. Kaiser et al. 2015 and Pearson et al. 2017 illustrate the great potential of SfM for this task. Furthermore, the authors might also refer to Woodget et al. 2018 regarding the usage of image texture and grain size estimation concerning most recent efforts in this regard because they use the original image instead of the potentially interpolated (and thus introducing further uncertainty) orthophoto.

References have been added to the paper to mention this option but we are not in a position to test the idea. Note that pixel size is of the same order as the D50 of the particle sizes so the textural effects on the DEM may be difficult to detect given the precision of elevation measurement. We also draw attention again to the differences between our small-scale rivers and the full scale UAV-based procedures referred to in the suggested papers.

Figures:

The figures involving flume display are very small and thus difficult to read and interpret. *These have been enlarged.*

References:

- Balaguer-Puiga, Matilde, Ángel, Marqués-Mateua, José Luis Lermaa, Sara, Ibáñez- Asensio (2017):, Geomorphology, 295
- Galland Olivier, Havard S. Bertelsen, Frank Guldstrand, Luc Girod, Rikke F. Johannessen, Fanny Bjugger, Stef Burchardt, and Karen Mair (2016): Application of open-source photogrammetric software MicMac for monitoring surface deformation in laboratory models, Journal of Geophysical Research: Solid Earth
- James, M. R. and Robson, S. (2014): Mitigating systematic error in topographic models derived from UAV and ground-based image networks, ESPL, 39
- James, M., Robson, S., Smith, M. (2017): 3-D uncertainty-based topographic change detection with structure-from-motion photogrammetry: precision maps for ground control and directly georeferenced surveys, ESPL, 42(12)
- James, MR, Robson, S, d'Oleire-Oltmanns, S and Niethammer, U (2017): Optimising UAV topographic surveys processed with structure-from-motion: ground control quality, quantity and bundle adjustment, Geomorphology, 280
- Javernick, L., Brasington, J., and Caruso, B. (2014): Modeling the topography of shallow braided rivers using Structure-from-Motion photogrammetry, Geomorphology, 213
- Kaiser, A., Neugirg, F., Haas, F., Schmidt, J., Becht, M., and Schindewolf, M. (2015): Determination of hydrological roughness by means of close range remote sensing, SOIL, 1
- Kaiser, Andreas, Annelie Erhardt, Anette Eltner (2018): Addressing uncertainties in interpreting soil surface changes by multitemporal high resolution topography data across scales, LDD
- Mosbrucker, Adam R., Jon J. Major, Kurt R. Spicer, John Pitlick (2017): Camera system considerations for geomorphic applications of SfM photogrammetry, ESPL, 42
- Pearson E., M.W. Smith, M.J. Klaar, L.E. Brown (2017): Can high resolution 3D topographic surveys provide reliable grain size estimates in gravel bed rivers? Geomorphology, 293
- Woodget, A. S., Carbonneau, P. E., Visser, F., and Maddock, I. P. (2015): Quantifying submerged fluvial topography using hyperspatial resolution UAS imagery and structure from motion photogrammetry, ESPL, 40
- Woodget, A., Fyffe, C., Carbonneau, P. (2018): From manned to unmanned aircraft: Adapting airborne particle size mapping methodologies to the characteristics of sUAS and SfM, ESPL, 43

Anonymous Referee 2

In this short communication, the authors detail Structure-from-Motion photogrammetry methods related to topographic measurements in a braided river flume experiment. The authors utilize automated batch processing to expedite creation of digital elevation models (DEMs) and provide a sampling of potential further analyses including the calculation of erosion and deposition using DEMs of difference (DoDs) and estimation of water depths. This study extends previous research on using Structure-from-Motion photogrammetry in laboratory flume settings and provides important insight that is relevant for researchers involved in similar physical experiments. The paper is straightfor-ward, logically organized, and easy to read. However, there are a few issues that need clarification or addressing. My primary concern is with the “error quantification” in Section 3.1. In subsection 3.1.1 DEMs derived from duplicate photosets of the same surface are compared to “estimate the mean and standard deviation of the vertical error” (P4, L7), while the comparisons of non-changing areas in subsection 3.1.2 are used to “estimate vertical precision” (P4, L15). I would consider the former to be a measure of precision also, rather than “error.” The use of the term “error” conveys the idea of comparison to a standard, or a measure of “trueness”, while these comparisons are between two surfaces of unknown accuracy. Subsection 3.1.3 does provide potential for actual error estimation, but the reported accuracy of the hand-held laser is not stated. A rewording of the parameters being estimated and quantified by the authors could strengthen section 3.1. I have more comments related to this section that will be included below.

Thank you for your comments. We have clarified the error/precision section.

Other comments:

P2, L13: Please also include the geometric standard deviation of the grain size distribution.

The geometric standard deviation of the grain size distribution is 1,4 mm. It has been added to the paper.

P3, L6: The guidance I have seen suggests having stationary lighting sources rather than one that moves with the camera (e.g., the camera flash). This does not seem to have negatively affected your results, but it is counter to general guidelines.

At first we considered using a stationary light as you mentioned but the flume is very close (less than a meter) to a white wall reflecting light. The resulting light would be not constant over the flume width and it is very difficult to get uniform light over an interior surface that is 3 x 18m. Previous experience demonstrate the shortcomings of this approach and we had more success with lights that move with the cameras to get a uniform and consistent light.

P3, L18: Was there general consistency in the density of the SfM point clouds? How did the point spacing compare to the DEM cell size and what was the interpolation method used to generate the DEMs?

The order of magnitude of the point cloud density was 80 points/cm², which correspond to 80 points for 45 DEM cells. We didn't notice density variations over time or space. We use the Photoscan interpolation (enabled option).

P4, L6: Please clarify, were the two photosets each made up of 100 photos (mentioned in P2, L24)?

Yes, each photo-set is made of 100 photos. We have clarified the text.

P4, L9: Was there a spatial pattern to the differences in the DoD maps (e.g., greater differences in areas with more complex topography)?

We didn't notice any consistent spatial pattern on the DoD. The DoD standard deviation seems to be linked to the picture quality (including picture overlap) rather than the bed complexity. Fig 1 (below) shows the mean difference on the DoD maps regarding to the bed standard deviation (we roughly consider that a smooth bed is likely associated to a low standard deviation and a complex bed is associated to a high standard deviation). The random shape of the point cloud indicates that there is no obvious trend between the DoD and the bed complexity. Furthermore, Figures 2 and 3 show an example of 2 different types of bed and the DoD associated, a smooth bed (Fig 2) and a complex bed (Fig 3). The DoD amplitude is in the order of magnitude of $d_{50} = 1.3\text{mm}$ (Fig. 2c and 3c). Dods (Fig. 2b and 3b) don't show any spatial pattern but subdued strips

(Fig. 3c) may be related to image overlap along the flume.

P4, L12: Were there any steps taken to ensure that the comparison to the DEM from the previous time did not include an area where geomorphic change may have taken place?

To choose a DEM we are using the DoD with the previous DEM. The DoD includes both the geomorphic changes and the measurement error – it is the nature of the experiment. The main hypothesis is that the error measurement would widen the elevation values of the DoD rather than narrow it. The chosen DEM is visually checked on the DoD and Dem plots.

P4, L18: The analysis in section 3.1.1 seems to be a better estimation of the “overall DEM noise” as the entire DEMs were used (< 1 mm, Table 1). Section 3.1.2 is a more localized analysis of DEM noise, where the greater variability (1 mm, Table 2) may be attributable to the featureless nature of the areas in the images used to generate the elevations of those “non moving, flat areas”. The analysis in this section does nicely highlight the effect of data collection improvement by the reduction in mean differences in Table 2.

We have revised the text to point this out.

P4, L21: What is the manufacturer/model of the laser scanner? What is its reported accuracy?

The TLS used is a Exascan scanner from Creaform. The resolution is 0.050 mm and the accuracy up to 0.040 mm. This has been added to the paper.

P4, L22: How were the scanner data oriented in real world coordinates? How did the point density from the laser scanner compare with SfM point density?

The hand-held laser scan point density was about half that of the SfM point cloud. Orientation is relative to the walls of the flume.

P5, L1: Was there any spatial pattern to the differences in the DEMs? What was the nature of the 30 cm x 39 cm area scanned (e.g., with or without channels/complex topography)?

*The bed 30 cm * 39 cm surface was in the side on the main channel and typical of the model topography in general. There were small bed elevation changes and it included channel margins and banks.*

P6, L5: What were Photoscan’s estimates for target errors? Were they consistent through time, or did they also improve?

The average target error from Photoscan was from 0,005 m to 0,001 m. The error is consistent within each experiment as targets are removed from the side of the flume each time the bed is flatten, ie at the end of each experiment.

P6, L14: The combining of DEMs described in subsection 3.1.1 is not derived from a single set of images. I’m not sure the last sentence of this paragraph is necessary or meaningful for how the data were processed.

The sentence is intended to point out that deriving 2 DEMs from separate image sets for each surface improves the probability of acquiring high quality topographic data. We say this to provide general advice and because our results show that in some cases one of the two surveys provides poorer quality data even though they are done one after the other using exactly the same conditions and setup. In other words there remains an element of unpredictability in quality despite this careful control – and this is useful for others to know in using this technique.

P6, L17: What are the specs of the machine used for processing (e.g., CPU, RAM)?

The specs of the machine are: 32GB RAM, Intel Core i7 processors (4790k) @ 4 GHz.

P7, L13: I suggest citing Wheaton et al. (2010a) and/or Wheaton et al. (2010b) in reference to Geomorphic Change Detection.

We now refer to their work.

P8, L6: Here you say images were collected in final minute of each experiment, but earlier (P6, L16) you say it took 15 minutes to collect the imagery?

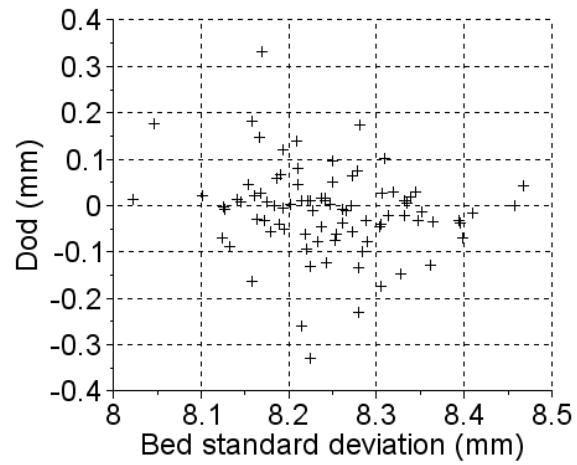


Figure 1: DoD precision versus topographic complexity of the bed

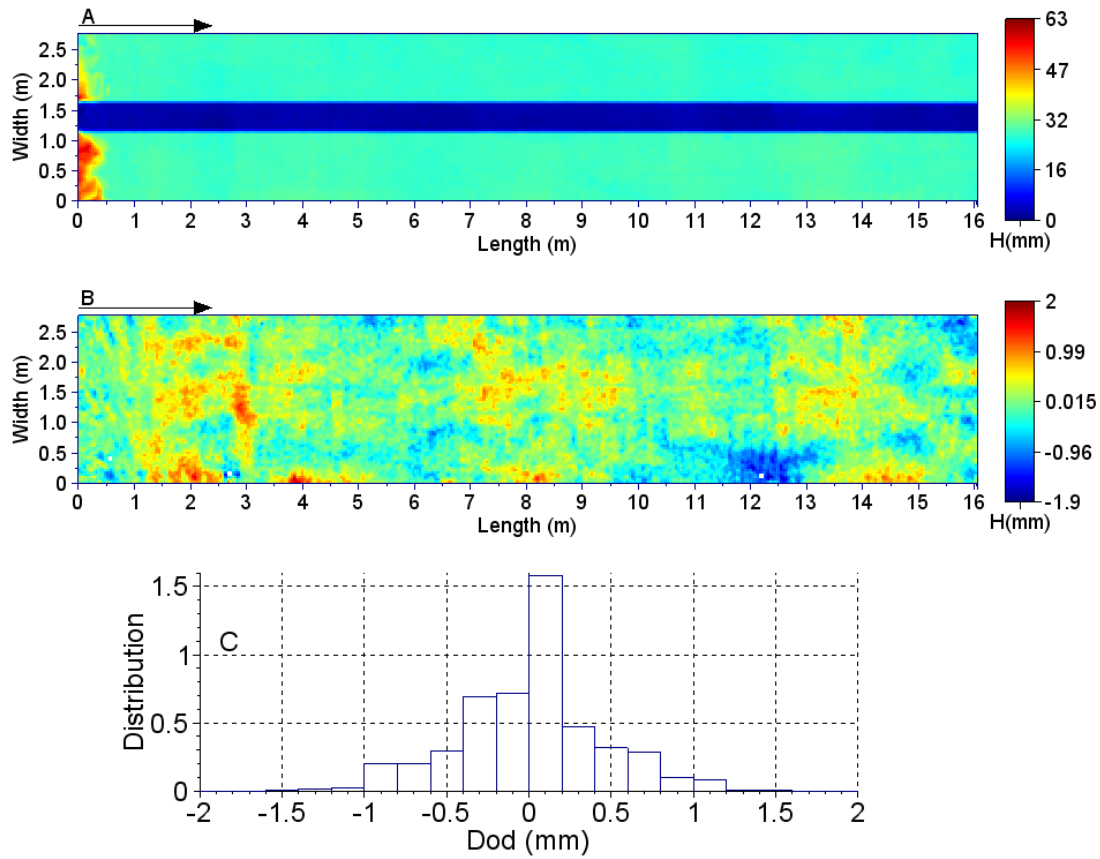


Figure 2: A relatively smooth and simple topography (a) with associated DoD of duplicate DEMs (b) and the DoD distribution (c)

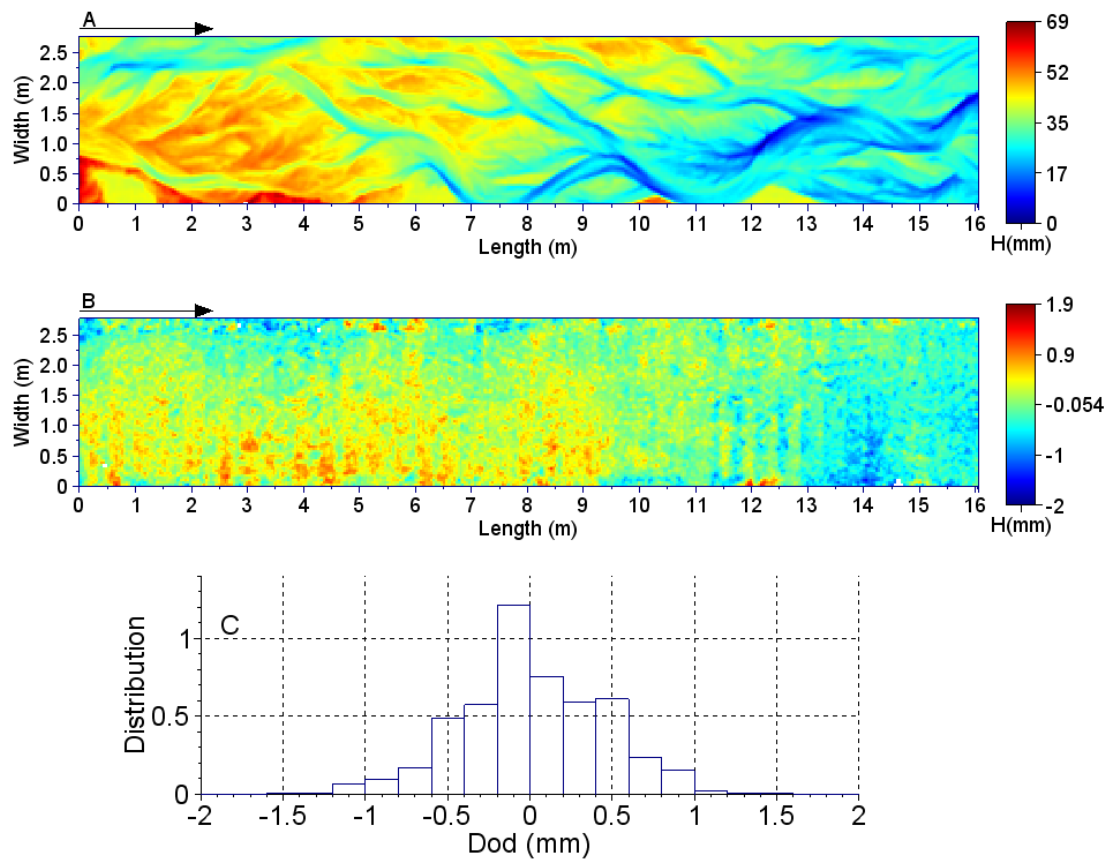


Figure 3: Example of a complex bed (a), the duplicate Dod (b) and the Dod distribution (c)

To estimate the water depth, the ‘wet’ set of picture was taken few minutes before the end of the 15 minute run. Only a short part of the flume was considered and only a single set of picture was taken. The number of pictures and thus the length on the wetted DEM was related to the time it took to collect the imagery.

P8, L10: How did derived depth maps compare with visual observations? Figure 7 looks like a single-thread channel. Was that the condition of the flume, or were there many other threads below the threshold of detection?

The method used only detected the deepest channels, mainly the active channels but the shallow channels aren’t well detected because flow is extremely shallow (a few mm).

P8, L11: Possibly make a recommendation or two for future development to improve your method.

We have added recommendations on the water surface detection.

P9, Figure 8B: Consider presenting the grain size data as a semi-log plot.

Easily done if required but range of particle sizes makes it unnecessary.

P12, L3: Please consider making your processing scripts (Python and Scilab) available also. You may be interested in also creating an entry on your methods/setup/equipment on Sediment Experimentalist Network (SEN) Knowledge Base (<http://sedexp.net/>).

The scripts and data will be available upon request. We will consider the Sediment Experimentalist Network.

Editorial comments:

All the editorial comments have been done.

P1, L22: “recent reports show the SfM techniques” should read “recent reports show that SfM techniques”

P2, L12: ‘2.71 s-1’ should be ‘2.71 m3s-1’

P4, Table 1 caption: “duplicates DEM” should be “duplicate DEMs”

P5, Table 2 caption: I think “Vertical precision” would be a more accurate description than “vertical error”

P5, L7: “Table 1” should be “Table 2”

P6, L12: “the focus as improved” should be “the focus was improved”

P9, L17: “different grain size” should be “different grain sizes”

P11, L5: “precision of the order” should be “precision on the order”

References:

Wheaton, J. M., J. Brasington, S. E. Darby, and D. A. Sear (2010a), Accounting for uncertainty in DEMs from repeat topographic surveys: improved sediment budgets, *Earth Surface Processes and Landforms*, 35 (2), 136-156, doi:10.1002/esp.1886.

Wheaton, J. M., J. Brasington, S. E. Darby, J. Merz, G. B. Pasternack, D. Sear, and D. Vericat (2010b), Linking geomorphic changes to salmonid habitat at a scale relevant to fish, *River Research and Applications*, 26 (4), 469-486, doi:10.1002/rra.1305.

Short Communication: Challenges and Applications of Structure-from-Motion Photogrammetry in a Physical Model of a Braided River

Pauline Leduc ¹, Sarah Peirce ¹, and Peter Ashmore ¹

¹Department of Geography, The University of Western Ontario, London, N6A 3K7, Canada

Correspondence: Peter Ashmore (pashmore@uwo.ca)

Abstract. Extending the applications of Structure-from-Motion (SfM) photogrammetry in river flumes, we present the main challenges and methods used to collect a large dataset (> 1000 digital elevation models) of high-quality topographic data using close-range SfM photogrammetry with a resulting vertical precision of ~ 1 mm. Automatic target-detection, batch processing, and considerations for image quality were fundamental to successful implementation of SfM on such a large dataset, which was used primarily for capturing details of gravel-bed braided river morphodynamics and sedimentology. While the applications of close-range SfM photogrammetry are numerous, we include sample results from DEM differencing, which was used to quantify morphology change and provide estimates of water depth in braided rivers, as well as image analysis for mapping bed surface texture. These methods and results contribute to the growing field of SfM applications in geomorphology and close-range experimental settings in general.

10 1 Introduction

Photogrammetric techniques have a long history in geomorphology, both in the field and laboratory, but the emergence of "Structure-from-Motion" (SfM) digital photogrammetry represents a technological revolution in geomorphological terrain analysis (~~Westoby et al., 2012; Tarolli, 2014; Bakker and Lane, 2017~~) (Westoby et al., 2012; Tarolli, 2014; Bakker and Lane, 2017; Javernick et al., 2014; Woodget et al., 2015). Unlike traditional methods which require a high level of expertise, a priori knowledge of camera positions, fixed and calibrated camera geometry, and/or the real-world 3D locations of ground control points (GCP), SfM allows camera positions and the geometry of a scene to be solved automatically and simultaneously (Westoby et al., 2012; Fonstad et al., 2013; Smith et al., 2016). In addition, the availability of inexpensive high-resolution digital cameras and user-friendly photogrammetric software to produce digital elevation models (DEMs) means that the resolution and quality of the DEMs is now primarily limited by quality of the input imagery (Chandler, 1999; Brasington and Smart, 2003; Rumsby et al., 2008). Fluvial geomorphologists are taking advantage of these advances and have used SfM photogrammetry to study rivers from large, dynamic braided rivers in the field to laboratory flumes and physical models (Kasprak et al., 2015; Leduc et al., 2015; Bakker and Lane, 2017; Morgan et al., 2016). While much of the research on SfM has been field-based (typically using unmanned automated vehicle, UAV,

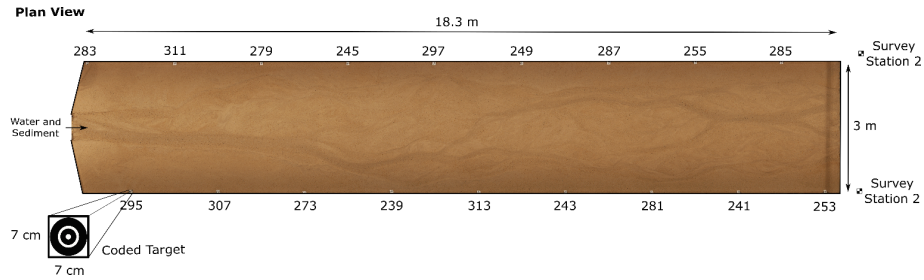


Figure 1. Planform view of the flume showing coded target locations and total station survey locations. Numbers refer to the unique target identifiers used in Agisoft PhotoScan’s automated target detection.

platforms) recent reports show ~~the~~ ~~that~~ SfM techniques have the potential provide a less expensive, but effective alternative to other methods such as laser scanning in close-range flume and laboratory settings (Kasprak et al., 2015; Morgan et al., 2016).

Here, we present methods for DEM and orthophotos acquisition from a Froude-scaled physical model of a gravel-bed braided river. We used close-range SfM techniques, enhanced with custom scripts for automatic control target detection and batch processing, to collect over 1000 high-quality DEMs of the 18.3 x 3 m model surface over a series of braided river experiments. While general guidelines for using close-range SfM have been discussed elsewhere (see Morgan et al. (2016)), here we address specific challenges faced and present methods used to improve data collection and the resulting data quality. We demonstrate that these techniques can be used to extract detailed morphological information, water surface topography and flow depth, as well as grain size/texture data from braided river models. These efforts contribute to the identified need for ongoing learning about application and quality of SfM in laboratory settings (Morgan et al., 2016).

2 Physical Model and Experimental Procedure

Data was gathered from small Froude-scaled physical models of braided gravel-bed rivers in a river modelling flume located at the The University of Western Ontario (UWO) (Fig. 1). The flume was 18.3 m long and 3 m wide with adjustable slope and discharge with a maximum of 2.5 % and $2.7 \text{ m} \cdot \text{s}^{-1}$, respectively. The grain size distribution ranged from 0.18 mm to 8 mm, with D_{10} of 0.32 mm, D_{50} of 1.18 mm, and D_{90} of 3.52 mm and a geometric standard deviation of 1.4 mm, representing the particle size distribution of the gravel fraction of a real gravel-bed braided river at an approximately 1:35 scale. The results presented come from a series of experiments covering six different stream power conditions to monitor morphological processes and variability over time. These experimental conditions extend the work of Morgan et al. (2016) into additional complex braided morphologies and graded grain size distributions.

Digital images of the model surface and bed topography were acquired from the drained bed (no standing water) at regular intervals of either 15 or 30 minutes, across six experiments that lasted between 29 and 68 hours each. Two sets of digital images (i.e. photo surveys) of the drained model surface were taken for every interval using two Canon T5i cameras (18 mega-pixel sensor with 20 mm lenses) stationed on a movable trolley. The trolley was situated on rails 2.7 - 2.9 m above

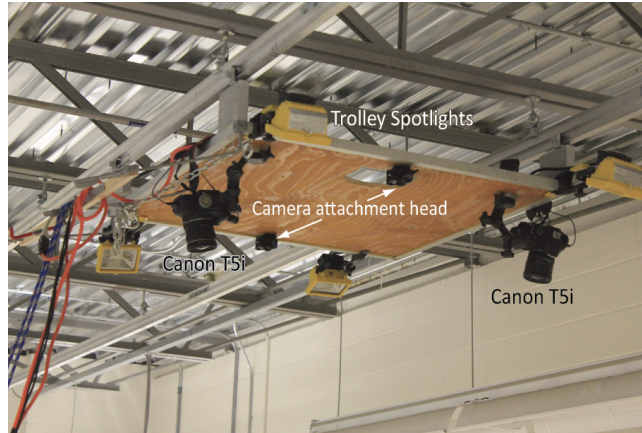


Figure 2. Movable trolley above model surface with 2 Canon cameras in a convergent position as well as four spotlights.

the model surface (Fig. 2) providing image coverage of the entire flume width. The cameras were positioned in a convergent geometry so that there was $\sim 80\%$ transverse overlap between photos over the center area of the model where morphological change was expected to be greatest. The trolley was pulled along the length of the flume with a longitudinal image overlap of $\sim 60\%$ across an average of 100 photos (50 photos from each camera) to cover the flume area. The cameras were triggered

5 simultaneously using the software DigiCamControl, which also allowed images to be downloaded directly to a computer. This camera positioning and geometry was consistent throughout all experimental runs following a more traditional near-vertical aerial photography geometry (Gardner and Ashmore, 2011; Kasprak et al., 2015; Leduc et al., 2015) than is sometimes the case for SfM applications, which may use images from multiple positions and angles (Morgan et al., 2016).

The two sets of digital images which don't have the same exact number of pictures, exact start and end locations and overlap, are used to estimate the precision of the survey (see section 3.1.1).

10

In addition to the dry bed photo surveys, additional wet bed photo surveys were acquired immediately prior to turning off the flow, when there was still water flowing in the model. These images were used to explore whether SfM could be used to map water surface topography in braided channels. During all photo surveys, spotlights attached to the camera trolley (Fig. 2) were used as the only light source to create consistent illumination of the model surface and minimize shadows and reflections

15 that can negatively impact photogrammetric outcomes.

3 DEM generation using SfM Digital Photogrammetry

The software package Agisoft PhotoScan 1.0.0.1 (i.e. PhotoScan) was used for digital photogrammetric processing to convert both the dry and wet bed photo surveys into a high-resolution DEM and orthophotos. While SfM allows for the creation of a dense point cloud without a priori knowledge of camera or target locations, reference to "real-world" position still requires

20 independent ground control points for georeferencing (Fonstad et al., 2013). Therefore, a dense control target array used 18 7 x 7 cm coded targets printed from Agisoft PhotoScan software placed on the inside walls of the flume via industrial Velcro

Experiment	μ (mm)	σ (mm)
1	0	0.4
4	0	0.2
9	- 1	0.2
11	- 1	0.6
12	0	0.3
13	0	0.2

Table 1. The mean value (μ) and the standard deviation (σ) of the vertical difference between ~~duplicates DEM~~ duplicate DEMs for each experiment

(Fig. 1). Target locations were independently surveyed for each of the six experiments using a total station from two survey station locations at the downstream end of the flume (Fig. 1) and converted into a text file of 3D (xyz) positions (sub-millimetre precision from repeat surveys) using 3D intersection. The target coordinates were used in the automatic target detection process in PhotoScan. This process was used to generate ~~1000 DEMs with a cell size of~~ DEM from a dense cloud with a density of 80
 5 points/cm² using the PhotoScan interpolation. The final cell size was 1.5 mm (close to the median grain size) and more than
1000 DEMs and orthophotos were generated.

3.1 ~~Error~~ Precision and error qualification from the DEM

Estimates of the vertical ~~error~~ precision in the DEMs in each experiment were calculated from multiple photo surveys of the same surface, and non-moving, flat areas. Elevation accuracy was also assessed by direct comparison with a local laser scan of
 10 a small area of the model surface.

3.1.1 Multiple photo surveys of the same surface

Two sets of dry bed photo surveys (approximately 100 pictures for each sets) were taken of the model surface at the end of each experimental run, and the resulting paired DEMs were used to estimate the mean and standard deviation of the vertical ~~error~~ precision (Table 1). In addition to the ~~error~~ precision quantification, the two DEMs of the same surface were compared
 15 so that only one DEM from each pair would be used for further analysis. For each pair of DEMs, a DEM of difference (DoD) was created. When the mean value of the DoD was less than 0.5 mm, preference was arbitrarily given to the first photo survey and DEM. If the difference in the paired DoD was greater than 0.5 mm, each DEM was then compared to the DEM from the previous time interval (for which the error decision was already made) and preference was given to the DEM providing the lowest mean value of elevation difference.

Experiment	σ (mm)
1	2.4
4	1.3
9	1.66
11	1.15
12	0.96
13	0.79

Table 2. Vertical ~~error~~ precision estimates for each experiment based on the standard deviation (σ) in the distribution of the elevations for the non-moving areas.

3.1.2 Non moving, flat areas

Flat, non-moving areas on the edges of the model surface, which were not reworked by the flow during the experiment, were also used to estimate the vertical precision across all DEMs within each experiment. This gives an estimate of precision for surfaces that are known not to have changed elevation between surveys and gives information on repeatability for the surveys.

- 5 The edge of the flat areas was defined by automatically detecting the slope break between the flat area and the channel bank in each row of the DEM. The error estimate was then calculated by differencing only the flat areas between two consecutive DEMs, and then merging the values within each experiment (Table 2). Based on this analysis, the overall DEM noise was around 1 mm, but noise was reduced in later experiments as data collection technique improved (Table 2).

3.1.3 Laser scan topography comparison

- 10 A final assessment of the data error compared a DEM produced from Agisoft PhotoScan to a DEM generated from a hand-held 3D surface laser scan ~~of the~~ (Exascan scanner from Creaform, with a resolution of 0.050 mm and the accuracy up to 0.040 mm.) of the same surface. The area scanned was about 30 cm * 39 cm which corresponds to over $50 * 10^3$ points. Figure 3 shows that the elevation distribution is roughly centred around 0 (mode= -0.08 mm) and fits a normal law ($\sigma = 0.62$, $\mu = -0.25$). Based on the distribution properties, the 99.7 % confidence interval of the difference is [-0.13 mm, 1.37 mm], which is again on the
- 15 scale of the D_{50} of the grain size in the flume.

4 Challenges: Improving data collection and outcomes in a laboratory flume

- While SfM offers speed, accuracy, and flexibility, there were several challenges encountered when applying close-range SfM techniques in the laboratory. As a result, the quality of the DEMs within and between the experiments was inconsistent. Based on Table ~~1~~ 2, in which the experiments are numbered in the order that they were completed, the data collection procedure and
- 20 quality of the resulting DEMs improved with experience and better understanding of the influences on DEM quality.

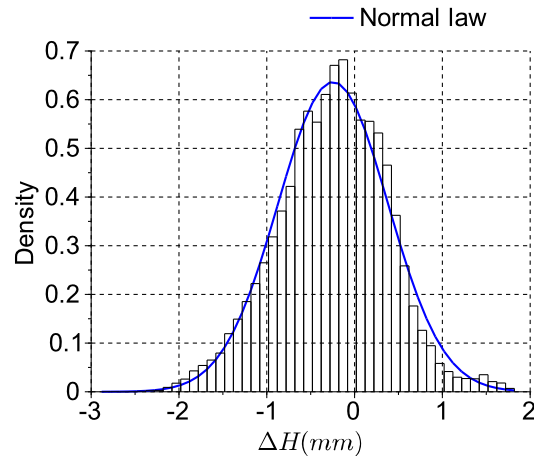


Figure 3. The elevation difference distribution comparing the DEM from Agisoft and the DEM generated using a Laser scan. The mean value is -0.25 mm (the mean absolute value is 0.53 mm) and the standard deviation is 0.62 mm (the mean absolute standard deviation is 0.43 mm).

4.1 The doming effect

Initial tests yielded some longitudinal doming in the DEMs which is often referred to in SfM literature (e.g., Kasprak et al., 2015; Smith et al., 2016; Morgan et al., 2016; James et al., 2017). A careful camera calibration using Agisoft Lens in addition to a stronger image convergence using the two cameras (James and Robson, 2014) eliminated the doming effect and no systematic error was noticed afterwards.

5 4.2 Target detection and camera settings

While SfM does not require target detection for dense-point cloud generation, the overall data quality was affected by the number of coded targets recognised by PhotoScan’s automated target detection during data processing. ~~In addition, initial tests yielded some longitudinal doming in the DEMs which is often referred to in SfM literature (e.g., Kasprak et al. (2015); Smith et al. (2016); Morgan et al. (2016)). In both cases, it~~ It was important to maximize the number of targets detected by adjusting target and camera positions accordingly and continually confirming that targets were being detected through visual analysis of each photo surveys. The convergent geometry of the two camera system may also be part of this solution, as has been reported in the past (Wackrow and Chandler, 2008; Smith et al., 2016) but we did not explicitly test this.

Image quality was also crucial to maximizing precision, as has been described (Mosbrucker et al., 2017). Superior camera focus was fundamental to SfM success and even a very slight "softness" in focus degraded DEM results considerably (Fig. 4) and in some cases made DEM results unusable. A fixed focal length lens was essential, especially in low light, close-range conditions, where the surface can have a uniform appearance in photos (Fig. 1) and fixed focal length aids sharpening of focus

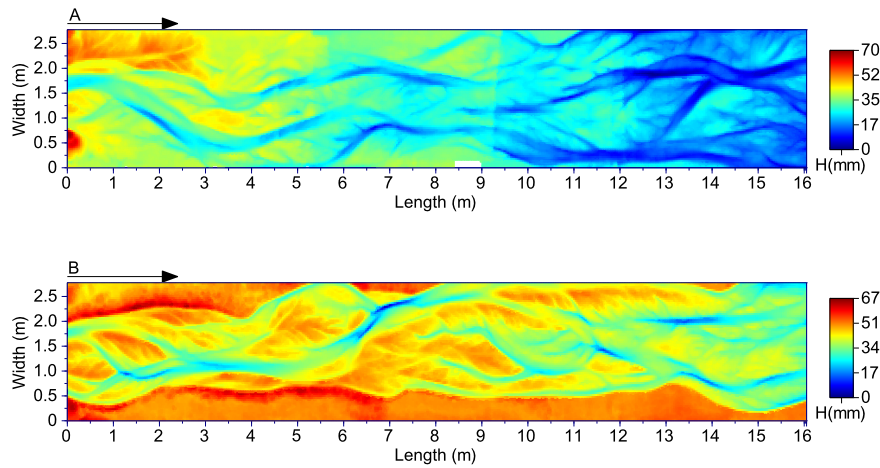


Figure 4. DEMs resulting from slightly out of focus images (A) compared to a DEM created under the same flow condition with superior focus (B).

[as well as improving geometric stability \(Mosbrucker et al., 2017\)](#). In later experiments, the focus ~~as was~~ improved during every photo survey by zooming in on small vector drawings placed in the field of view. Finally, capturing two photo surveys for each surface improved the probability of acquiring at least one set of high quality images and overall improved DEM results.

4.3 Processing time

Each photo survey (i.e., one set of images of the full flume length) took approximately 15 minutes to collect and approximately 5 hours of processing time in PhotoScan to generate a high-resolution DEM and orthophoto. To ensure that the data were processed continually, a simple Python script was written that allowed for batch processing of the photo surveys. The input for the script was the images from the photo surveys, coded target locations, and initial camera calibration parameters derived by PhotoScan. While the processing was time consuming, the automation made it possible to continuously process photos and generate >1000 high-resolution DEMs (~ 500 unique model surfaces) across all six experiments over a few months which was at least an order of magnitude faster than manual target acquisition and processing with older digital photogrammetry software (~~e.g. Gardner and Ashmore (2011)~~). [\(e.g., Gardner and Ashmore, 2011\)](#). The output of the batch processing script was an orthophoto and a DEM of the flume surface with 1.5 mm pixels. The script additionally exported a report on the PhotoScan project, indicating the number of photos used, the image overlap, and the estimated error on target detection. Morgan et al. (2016) reported that they were unable to utilize the automated target detection feature in PhotoScan but our fixed geometry and consistent survey method may have been important to successful automated target identification. Furthermore, it was found that using large identification values on the targets (e.g., ID numbers > 100 (see Fig. 1)) helped to avoid PhotoScan confusing targets signals during processing, which also improved overall batch processing success.

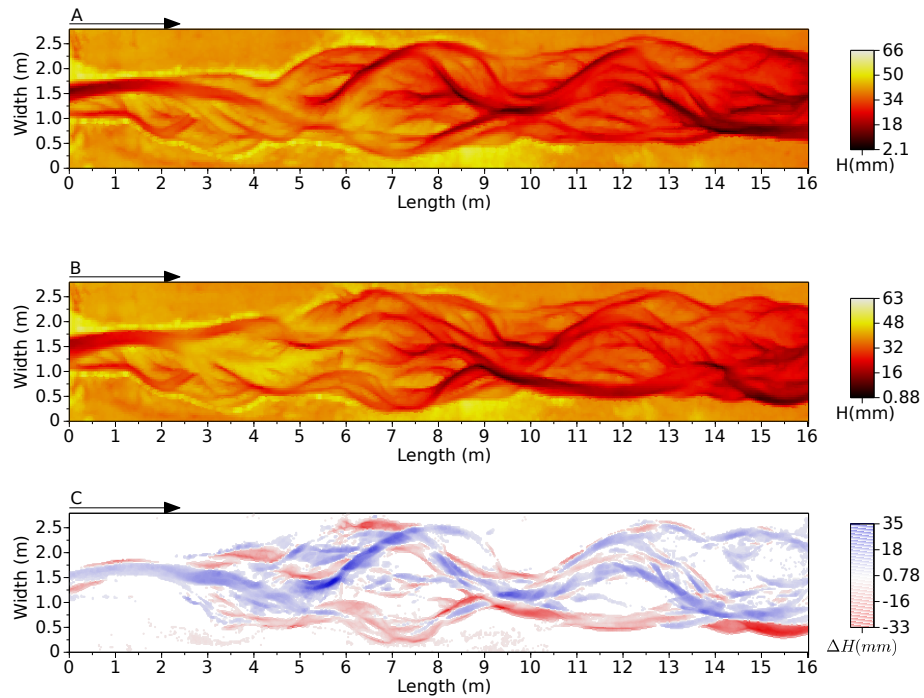


Figure 5. Generation of a DEM of Difference (DoD) using two consecutive DEMs where (A) DEM2 (time = 1200 min) was subtracted from (B) DEM1 (time = 1400 min) to create a (C) DoD where areas of erosion are red and areas of deposition are blue.

5 Applications in Braided River Geomorphology

15 5.1 DEMs and DEMs of Difference

Examples of the final DEMs and DEMs of difference (DoDs) are shown in Fig. 5. From the batch processed DEMs there was flexibility in post-processing (using custom Scilab scripts) for cropping, filtering, and change detection thresholds for various geomorphic analyses including extracting both the areas and volumes of erosion and deposition. An alternative to using custom scripts would be the software program Geomorphic Change Detection ([Wheaton et al., 2010a, b](#)) or ArcGIS, although a comparison of techniques was not completed for this research. In addition to estimating changes in the morphological active width (Peirce et al., 2018a), the data can be used for many applications, including estimates of water depth and bed surface texture.

5.2 Water Depth

Estimation of water depths and water surface slope is valuable in small scale models of complex planform where direct measurement and synoptic mapping of water depth are very difficult due to shallow (~ 2 cm) depths and constantly changing

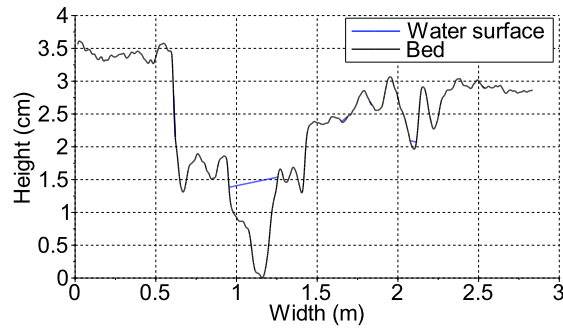


Figure 6. Example of water surface detection. In the cross section, we assume a straight line between the first water point (i.e. the difference is higher than the threshold) on the cross section and the first next dry point (i.e. the difference is lower than the threshold).

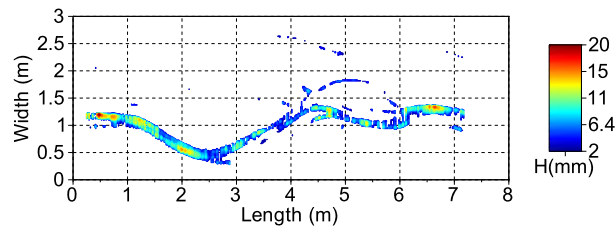


Figure 7. Example of a water depth map for a small (8m) reach of the flume.

5 morphology. Detection of the water surface was possible by creating a DoD from the water surface DEM and matching dry bed DEM for a given time period interval (Fig. 6).

The photo surveys of the water surface were taken in the final minute of each experiment to avoid morphological change between the subsequent dry bed photo surveys. In the DoD, only change greater than 1 mm (approximate mean error through all the experiments, Table 2) was considered and it was assumed that differences detected were the result of water depth and not morphological change (Fig. 6). From this data, a binary map (water/non water) was created and the elevation of the water on a cross-section was taken to be the elevation of the closest non-water cell. For this analysis, it was assumed that the water level was straight at the cross-sectional scale, and a water depth map ~~is~~ was extracted from the cross section analysis (Fig. 7).

The techniques used requires refinement and further assessment but presents an important area for future development of SfM methods in laboratory models and flumes.

15 Validation is currently problematic because water depth is not measured directly. This could be improved if it was possible to make a direct comparison between water surface and bed elevation at a point.

5.3 Bed Surface Texture

Maps and data of the grain size distribution and bed surface texture can be used for a variety of analyses but their immediate value is in showing the wide range, and spatial patterns, of texture (grain size) on the gravel braided river model bed surface.

20 Previous papers based on experiments in the same flume and sediment have shown that maps of bed surface texture, as a measurement of grain size variation, may be produced from the same imagery created for the photogrammetry.

Grain size For bed material larger than the cell size, SfM may be an alternative method to estimate the bed grain size using the DEM surface roughness, and correlating the standard deviation of elevations with particle diameters Pearson et al. (2017). This is likely to be less successful when grain roughness is less than the precision of the DEMs and pixel sizes are approximately equal to median particle diameter as in this close-range application in a small-scale flume model.

5 For medium sand we used, grain size analysis and mapping was based on the image texture method developed and tested by Carbonneau (2005) and Carbonneau et al. (2005) for field mapping of gravel-bed rivers and previously adapted for the sand texture of physical models (Gardner and Ashmore, 2011; Leduc et al., 2015). The image texture calculation was made using the co-occurrence gray matrix level based on 64 gray level vertical bed images. The sampling window size of 7 * 7 pixels was chosen due to the median grain size (1.3 mm) and the camera resolution, and the best fit of the data was found using the entropy index. To calibrate the predictive relationship between an entropy value and the real grain size, two sets of samples were used.

The first was based on the surface grain size samples from the Sunwapta River, Canada (a gravel-bed braided river from which the flume grain size distribution was based) and the second was based on uniform grain size patches from the flume bed material. The field calibration dataset was generated from 13 grain size samples randomly selected from a larger dataset of 30 samples. The field samples were manually sieved using an adaptation of the paint-and-pick technique, where a chalk dot was drawn on every visible surface grain. The 13 grain size samples were downsampled to get the calibration grain size sample composition. In addition to the non-uniform field samples, 6 uniform samples were also created from the different grain sizes of the bed material.

In total, ~~theses~~ these 19 samples covered the full range of grain size in the flume (Fig. 8 A). For the flume calibration dataset, grains were mixed and glued to a white foam board in a continuous thick layer with an area of 10 cm * 15 cm (Fig. 8 B). The sampling board was placed on the flume bed at different locations and the entropy value was estimated for each sample at each location over a square of $\sim 3.7\text{cm}^2$. Each sample represented over 5000 pixels on the picture. The final flume calibration relationship was built using the median grain size of the sample and the corresponding entropy value (Fig. 9).

5 In addition to the calibration datasets, a validation dataset was created from 100 grain samples on the flume bed, collected using 1cm^2 wax drops poured directly onto the bed (Fig. 10) and manually sieved. On the corresponding orthophotos (Fig.10), the centre of each wax drop was manually set and the entire wax drop surface was automatically detected using a color threshold. Of the initial 100 wax samples, 70 were used for validation. The measured grain size was compared to the entropy maps generated from the texture calculation (Fig. 11) and for which the mean absolute error was 0.02 mm with a standard deviation of 0.48 mm, although the relative error was higher for smaller grains.

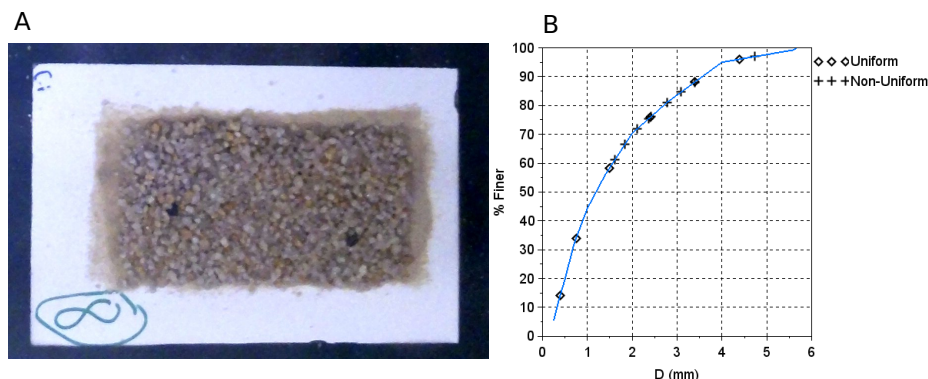


Figure 8. (A) An example of calibration sample used during the calibration of the bed surface texture, and (B) the median grain size of the calibration data samples, including uniform and non-uniform samples. The line is the flume grain size distribution.

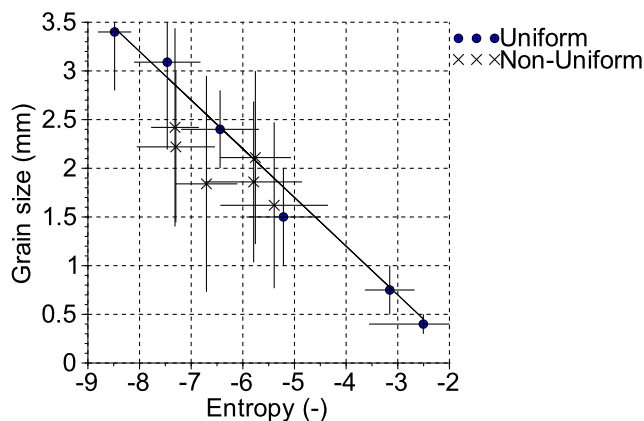


Figure 9. The grain size calibration for uniform and non-uniform samples. Horizontal error bars are the entropy standard deviation of the sample and the vertical bars are the grain size sieving range.

We refer to the estimated grain size from the textural calibration as the "equivalent texture" because it is a texture value calibrated to only the median grain size (not the full distribution) for a patch and is not strictly a grain size value as conventionally defined in physical measurements of grain size. A final grain size map was created for each DEM, mapping the bed elevation and local bed texture for the entire model surface (Fig. 12). Combining grain maps derived from orthoimagery, with DEMs and DoDs can provide data on, for example, bed roughness and changes over time, grain size sorting for sedimentological analysis and relations to bed morphology, and relationship to topographic roughness.

5.4 Application in geomorphology analysis

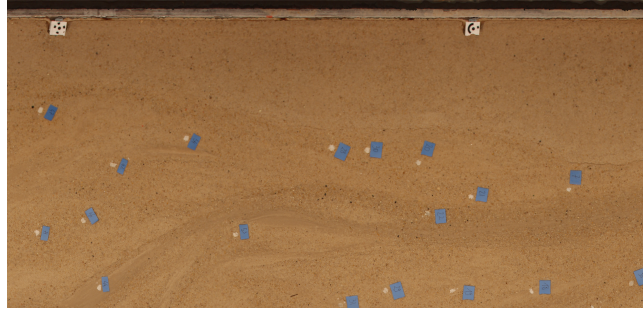


Figure 10. Image of the flume surface with the location of wax samples used for grain size validation.

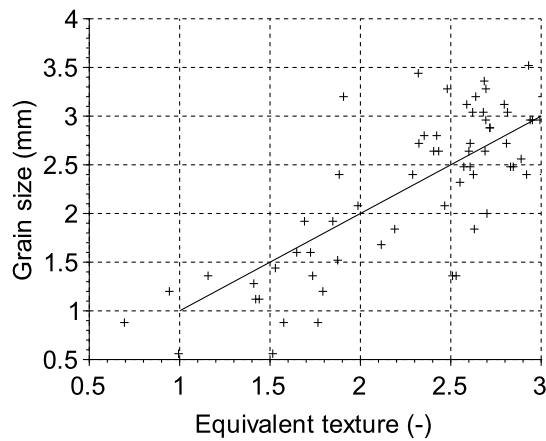


Figure 11. The validation dataset: the grain size from the texture analysis regarding the hand picked grain sizing.

10 [The SfM technology applied to our flume experiments provides more than 1000 DEMs and orthophotos which leads to an extensive geomorphological processes analysis. Based on these DEMs, studies focusing on the active width, planform evolution, grain size distribution and variability at a high temporal resolution \(see Middleton et al. \(2018\); Peirce et al. \(2018a, b\)\) are providing new insights on braided river morphology, dynamics and bedload transport.](#)

15 6 Conclusions

This paper presented methods for the successful application of SfM photogrammetry using Agisoft PhotoScan in a physical model of a gravel-bed braided river. Consideration of camera geometry, automated control-target detection, image quality, and batch processing made it possible to create a large number (>1000) of high-resolution DEMs of complex braided channel morphology with vertical precision ~~of~~ on the order of 1 mm. These DEMs can be used extensively, including to map and

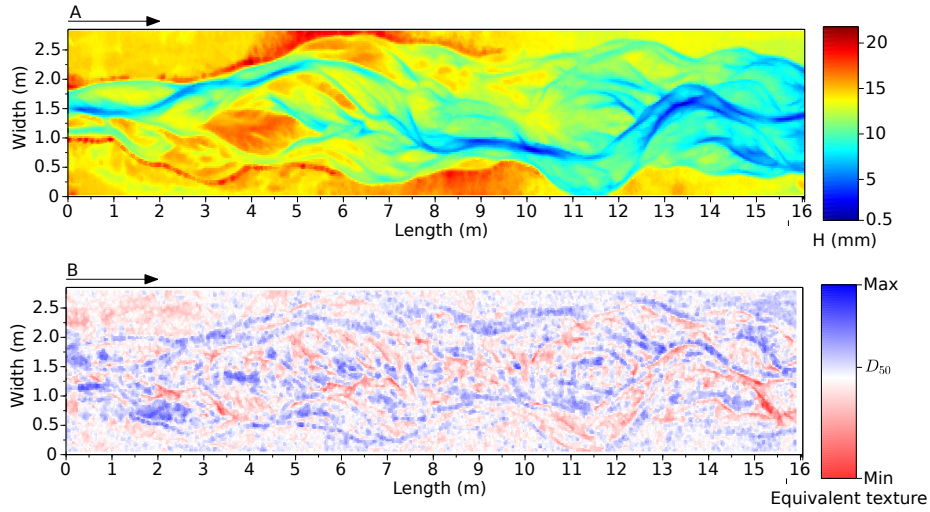


Figure 12. An example DEM (A) plotted with its associated equivalent texture map (B).

20 quantify morphological change (using DEMs of difference) as well as to acquire water surface DEMs to map wetted areas
 and estimate water depth. Additionally, the images collected can be used for mapping grain size variation across the braided
 river. The results presented demonstrate that SfM can yield large volumes of very high quality topographic data efficiently in
 close-range laboratory applications. In this way we have extended collective learning about the quality of SfM data acquisition
 methods in this type of laboratory setting and model (Morgan et al., 2016) and added to the range of conditions to which this
 25 technology has been applied.

Data availability. The data presented in the figures of this paper are available from the corresponding author.

Acknowledgements. This research was supported by a Natural Sciences and Engineering Research Council Discovery Grant (41186-2012)
 to P. Ashmore. Flume construction was supported by the Canada Foundation for Innovation and Newalta Resources Inc. Additional support
 was provided by the Vanier Canada Graduate Scholarship awarded to S. Peirce. Thank you to everyone who assisted with data collection,
 30 especially L.Middleton and D. Barr.

References

- Bakker, M. and Lane, S. N.: Archival photogrammetric analysis of river–floodplain systems using Structure from Motion (SfM) methods, *Earth Surface Processes and Landforms*, 42, 1274–1286, <https://doi.org/10.1002/esp.4085>, 2017.
- Brasington, J. and Smart, R.: Close range digital photogrammetric analysis of experimental drainage basin evolution, *Earth Surface Processes and Landforms*, 28, 231–247, <https://doi.org/10.1002/esp.480>, 2003.
- 35 Carbonneau, P. E.: The threshold effect of image resolution on image-based automated grain size mapping in fluvial environments, *Earth Surface Processes and Landforms*, 30, 1687–1693, 2005.
- Carbonneau, P. E., Bergeron, N., and Lane, S. N.: Automated grain size measurements from airborne remote sensing for long profile measurements of fluvial grain sizes, *Water Resources Research*, 41, <https://doi.org/10.1029/2005WR003994>, <http://dx.doi.org/10.1029/2005WR003994>, w11426, 2005.
- 5 Chandler, J.: Effective application of automated digital photogrammetry for geomorphological research, *Earth Surface Processes and Landforms*, 24, 51–63, [https://doi.org/10.1002/\(SICI\)1096-9837\(199901\)24:1<51::AID-ESP948>3.0.CO;2-H](https://doi.org/10.1002/(SICI)1096-9837(199901)24:1<51::AID-ESP948>3.0.CO;2-H), [http://doi.wiley.com/10.1002/\(SICI\)1096-9837\(199901\)24:1{ }3C51::AID-ESP948{ }3E3.0.CO;2-H](http://doi.wiley.com/10.1002/(SICI)1096-9837(199901)24:1{ }3C51::AID-ESP948{ }3E3.0.CO;2-H), 1999.
- Fonstad, M. A., Dietrich, J. T., Courville, B. C., Jensen, J. L., and Carbonneau, P. E.: Topographic structure from motion: A new development in photogrammetric measurement, *Earth Surface Processes and Landforms*, 38, 421–430, <https://doi.org/10.1002/esp.3366>, 2013.
- 40 Gardner, J. T. and Ashmore, P.: Geometry and grain-size characteristics of the basal surface of a braided river deposit, *Geology*, 39, 247–250, <https://doi.org/10.1130/G31639.1>, <http://geology.gsapubs.org/cgi/doi/10.1130/G31639.1>, 2011.
- [James, M. R. and Robson, S.: Mitigating systematic error in topographic models derived from UAV and ground-based image networks, *Earth Surface Processes and Landforms*, 39, 1413–1420, 2014.](#)
- 15 [James, M. R., Robson, S., d’Oleire Oltmanns, S., and Niethammer, U.: Optimising UAV topographic surveys processed with structure-from-motion: Ground control quality, quantity and bundle adjustment, *Geomorphology*, 280, 51–66, 2017.](#)
- [Javernick, L., Brasington, J., and Caruso, B.: Modeling the topography of shallow braided rivers using Structure-from-Motion photogrammetry, *Geomorphology*, 213, 166–182, <https://doi.org/10.1016/j.geomorph.2014.01.006>, <http://dx.doi.org/10.1016/j.geomorph.2014.01.006>, 2014.](#)
- 20 Kasprak, A., Wheaton, J. M., Ashmore, P., Hensleigh, J. W., and Peirce, S.: The relationship between particle travel distance and channel morphology : Results from physical models of braided rivers, *Journal of Geophysical Research F: Earth Surface*, 120, 55–74, <https://doi.org/10.1002/2014JF003310>.Received, 2015.
- Leduc, P., Ashmore, P., and Gardner, J. T.: Grain sorting in the morphological active layer of a braided river physical model, *Earth Surface Dynamics*, 3, 577–585, <https://doi.org/10.5194/esurf-3-577-2015>, 2015.
- 25 [Middleton, L., Ashmore, P., Leduc, P., and Sjogren, D.: Rates of planimetric change in a proglacial gravel-bed braided river: field measurement and physical modeling, *Earth Surface Processes and Landforms*, <https://doi.org/10.1002/esp.4528>, 2018.](#)
- Morgan, J. A., Brogan, D. J., and Nelson, P. A.: Application of Structure-from-Motion photogrammetry in laboratory flumes, *Geomorphology*, 276, 125–143, <https://doi.org/10.1016/j.geomorph.2016.10.021>, <http://dx.doi.org/10.1016/j.geomorph.2016.10.021>, 2016.
- [Mosbrucker, A. R., Major, J. J., Spicer, K. R., and Pitlick, J.: Camera system considerations for geomorphic applications of SfM photogrammetry, *Earth Surface Processes and Landforms*, 42, 969–986, <https://doi.org/10.1002/esp.4066>, 2017.](#)

- 265 [Pearson, E., Smith, M., Klaar, M., and Brown, L.: Can high resolution 3D topographic surveys provide reliable grain size estimates in gravel bed rivers?, *Geomorphology*, 293, 143–155, <https://doi.org/10.1016/j.geomorph.2017.05.015>, <http://dx.doi.org/10.1016/j.geomorph.2017.05.015><http://www.sciencedirect.com/science/article/pii/S0169555X17302404>, 2017.](#)
- Peirce, S., Ashmore, P., and Leduc, P.: The ~~Variability in the Morphological Active Width~~[variability in the morphological active width: Results from ~~Physical Models of~~ physical models of gravel-bed braided rivers, *Earth Surface Processes and Landforms*, 43, 2371–2383, <https://doi.org/10.1002/esp.4400>, 2018a.](#)
- 270 [Peirce, S., Ashmore, P., and Leduc, P.: Evolution of Grain Size Distributions and Bed Mobility during Hydrographs in Gravel-Bed Braided Rivers, *Earth Surface Processes and Landforms*, -, 2018-<https://doi.org/10.1002/esp.4511>, 2018b.](#)
- Rumsby, B., Brasington, J., Langham, J., McLelland, S., Middleton, R., and Rollinson, G.: Monitoring and modelling particle and reach-scale morphological change in gravel-bed rivers: Applications and challenges, *Geomorphology*, 93, 40–54, <https://doi.org/10.1016/j.geomorph.2006.12.017>, <http://linkinghub.elsevier.com/retrieve/pii/S0169555X07001547>, 2008.
- 275 [Smith, M. W., Carrivick, J. L., and Quincey, D. J.: Structure from motion photogrammetry in physical geography, *Progress in Physical Geography*, 40, 247–275, <https://doi.org/10.1177/0309133315615805>, <http://ppg.sagepub.com/content/40/2/247.abstract?rss=1>, 2016.](#)
- Tarolli, P.: High-resolution topography for understanding Earth surface processes: Opportunities and challenges, <https://doi.org/10.1016/j.geomorph.2014.03.008>, 2014.
- Wackrow, R. and Chandler, J. H.: A convergent image configuration for DEM extraction that minimises the systematic effects caused by an
280 inaccurate lens model, *The Photogrammetric Record*, 23, 6–18, <https://doi.org/10.1111/j.1477-9730.2008.00467.x>, <https://onlinelibrary.wiley.com/doi/abs/10.1111/j.1477-9730.2008.00467.x>, 2008.
- Westoby, M. J., Brasington, J., Glasser, N. F., Hambrey, M. J., and Reynolds, J. M.: 'Structure-from-Motion' photogrammetry: A low-cost, effective tool for geoscience applications, *Geomorphology*, 179, 300–314, <https://doi.org/10.1016/j.geomorph.2012.08.021>, <http://linkinghub.elsevier.com/retrieve/pii/S0169555X12004217>, 2012.
- 285 [Wheaton, J. M., Brasington, J., Darby, S. E., Merz, J., Pasternack, G. B., Sear, D., and Vericat, D.: Linking geomorphic changes to salmonid habitat at a scale relevant to fish, *River Research and Applications*, 26, 469–486, <https://doi.org/10.1002/rra.1305>, 2010a.](#)
- [Wheaton, J. M., Brasington, J., Darby, S. E., and Sear, D. A.: Accounting for uncertainty in DEMs from repeat topographic surveys: Improved sediment budgets, *Earth Surface Processes and Landforms*, 35, 136–156, <https://doi.org/10.1002/esp.1886>, 2010b.](#)
- 290 [Woodget, A. S., Carbonneau, P. E., Visser, F., and Maddock, I. P.: Quantifying submerged fluvial topography using hyperspatial resolution UAS imagery and structure from motion photogrammetry, *Earth Surface Processes and Landforms*, 40, 47–64, <https://doi.org/10.1002/esp.3613>, 2015.](#)